Preparation and Characterization of Exfoliated Layered Double Hydroxide/Silicone Rubber Nanocomposites

Bratati Pradhan,[1] Suneel Kumar Srivastava,[1] Rajakumar Ananthakrishnan,[1] Anubhav Saxena[2]

[1]*Department of Chemistry, Indian Institute of Technology, Kharagpur, India 721302*
[2]*Momentive Performance Materials Programs, GE India Technology Centre Private, Limited, Bangalore, India 560 066*

Received 24 December 2009; accepted 12 April 2010
DOI 10.1002/app.32614
Published online 27 July 2010 in Wiley Online Library (wileyonlinelibrary.com).

ABSTRACT: Silicone rubber (SR)/Mg–Al layered double hydroxide (LDH) nanocomposites were prepared by the solution intercalation of SR crosslinked by a platinum-catalyzed hydrosilylation reaction into the galleries of dodecyl sulfate intercalated layered double hydroxide (DS–LDH). X-ray diffraction and transmission electron microscopy analysis showed the formation of exfoliated structures of organo-modified LDH layers in the SR matrix. The tensile strength and elongation at break of SR/DS–LDH (5 wt %) were maximally improved by 53 and 38%, respectively, in comparison with those of the neat polymer. Thermogravimetric analysis indicated that the thermal degradation temperature of the exfoliated SR/DS–LDH (1 wt %) nanocomposites at 50% weight loss was 20°C higher than that of pure SR. Differential scanning calorimetry analysis data confirmed that the melting temperature of the nanocomposites increased at lower filler loadings (1, 3, and 5 wt %), whereas it decreased at a higher filler loading (8 wt %). The relative improvements in the solvent-uptake resistance behavior of the SR/DS–LDH nanocomposites were also observed. © 2010 Wiley Periodicals, Inc. J Appl Polym Sci 119: 343–351, 2011

Key words: mechanical properties; nanocomposites; thermal properties

INTRODUCTION

In recent years, organic/inorganic polymers and inorganic material nanocomposites have attracted great attention in many promising fields of research because of their unique properties (e.g., improved mechanical, thermal, and gas-barrier properties and reduced flammability).[1–5] The improvements in these properties versus the neat polymers are strongly influenced by both the dispersion nature and compatibility of the nanofillers in the polymer matrix.[6] However, most research work has been focused on naturally occurring clays such as montmorillonite.[7] On the contrary, layered double hydroxides (LDHs), also known as anionic clays, have been studied relatively little because of the stronger interactions between the hydroxide sheets, small gallery space,[8] and hydrophilic nature of LDHs.[9] However, because of their extensive applications (e.g., catalysts, flame retardants, and medical materials) and highly tunable properties, LDHs are considered a new emerging class of materials used in the preparation of multifunctional polymer nanocomposites.[1,2,10,11] The LDH structure consists of stacks of positively charged mixed metal oxide/hydroxide layers that require the presence of interlayer exchangeable anions to maintain overall charge neutrality. The most important group of LDHs may be represented by the ideal formula:

$$[M^{2+}_{(1-x)}M^{3+}_{x}(OH)_2]A^{n-}_{x/n} \cdot mH_2O$$

where M^{2+} is a divalent cation (e.g., Mg^{2+}, Zn^{2+}, or Ni^{2+}), M^{3+} is a trivalent cation (e.g., Al^{3+}, Cr^{3+}, or Fe^{3+}), x is the ratio of M^{3+} to $M^{2+} + M^{3+}$, and A is an anion of valence n (e.g., Cl^-, CO_3^{2-}, SO_4^{2-}, or NO_3^-). The small basal spacing of pristine LDHs ($\sim$ 0.76 nm)[12] restricts the insertion of polymer chains, so appropriate surface modification is needed.[2] Depending on the degree of dispersion of the modified LDH layers in the polymer matrix, exfoliated, intercalated, and exfoliated–intercalated nanocomposites can be prepared. Interestingly, in exfoliated nanocomposites, the individual LDH layers are homogeneously dispersed in the polymer matrix with a very large polymer/filler interface, and this results in excellent improvements in the physicochemical properties.[2,6]

Silicone rubber (SR) possesses excellent weatherability, good chemical stability, oxidation resistance,

Correspondence to: S. K. Srivastava (sunit@chem.iitkgp.ernet.in).

Contract grant sponsors: Council of Scientific and Industrial Research, Department of Science and Technology, Defence Research and Development Organisation.

thermal stability, low-temperature toughness, electrical-insulation properties, low surface energy, low toxicity, and high optical transparency.[13] As a result, it is widely used for different applications such as lubricants, sealants, adhesives, medical implants, and electrical-insulation products.[14] However, an unfilled silicone elastomer usually has poor mechanical properties and low thermal/electrical conductivity, and these properties are likely to be improved by the reinforcement of SR with various inorganic nanofillers. According to the available literature, aerosilica is one of the most commonly used nanofillers in the SR industry.[15] However, because of its expense, easy agglomeration, and health hazards, attention has been focused on many other nanofillers, such as organomodified montmorillonite, hyperbranched organomontmorillonite, nanosilica, carbon black, carbon nanotubes, graphite, and nanohydroxyapatite.[16–18] However, the development of SR nanocomposites with other available nanofillers still remains unexplored. Therefore, this work deals with the synthesis of SR/dodecyl sulfate intercalated layered double hydroxide (DS–LDH) nanocomposites by a solution-intercalation method and their characterization by *X*-ray diffraction (XRD), transmission electron microscopy (TEM), and scanning electron microscopy (SEM). We have studied the mechanical properties, thermal stability, polymer crystallinity, and swelling properties of these SR/LDH nanocomposites.

EXPERIMENTAL

Materials

The commercially available SR Baysilone U10 (vinyl content = 0.05 mmol/g), a vinyl-terminated, linear polydimethylsiloxane base polymer, and the crosslinking agent Baysilone U430, a polysiloxane containing silicone-bonded hydrogen atoms, as well as a Pt catalyst complex were supplied by Momentive Performance Materials (Bangalore, India). Ethynyl cyclohexanol was purchased from Sigma–Aldrich (Steinheim, Germany) and used as an inhibitor. $Mg(NO_3)_2{\cdot}6H_2O$, $Al(NO_3)_3{\cdot}9H_2O$, Na_2CO_3, and carbon tetrachloride (CCl_4) were purchased from E. Merck (Mumbai, India). Sodium hydroxide (NaOH) and sodium dodecyl sulfate (SDS) were obtained from Quest Chemicals (Kolkata, India) and SRL (Mumbai, India), respectively, to prepare DS–LDH.

Sample preparation

Preparation of Mg–Al LDH

Mg–Al LDH was prepared according to the coprecipitation method.[19] $Mg(NO_3)_2{\cdot}6H_2O$ (0.25 mol, 19.65 g) and $Al(NO_3)_3{\cdot}9H_2O$ (0.75 mol, 9.25 g) were first dissolved completely in 100 mL of H_2O and added dropwise to an aqueous solution containing 0.25 mol (2.65 g) of Na_2CO_3 and 0.2 mol (8.00 g) of NaOH with stirring; the pH was maintained at 8–9 with an aqueous 1*M* NaOH solution. The white mass so obtained was subsequently aged for 16 h at 80°C, and this was followed by filtration and washing with distilled water. Finally, the product was dried under the ambient conditions for 24 h, and this was followed by vacuum drying at 80°C for 24 h. Mg–Al LDH (5 g) was calcined at 500°C for 6 h and dispersed at room temperature in a 200-mL aqueous solution in which 4 g of SDS had already been dissolved. The temperature was then increased to 80°C while stirring was continued for 12 h, and this was followed by refluxing at 100°C for 6 h. This resulted in the formation of a white product of organophilic LDH (DS–LDH), which was filtered and washed several times with distilled water to make it free from the surfactant.

Preparation of the SR nanocomposites

SR/DS–LDH nanocomposites with various amounts of DS–LDH (1, 3, 5, and 8 wt %) were prepared by solution blending. For this, the desired amount of DS–LDH was first dispersed in 25 mL of CCl_4 at 80°C for 6 h and added to a solution of 10 g of SR dissolved in 25 mL of CCl_4. The resultant mixture was stirred at 80°C for 8 h, and this was followed by the addition of appropriate amounts of the catalyst, inhibitor, and crosslinker (V430) with a 3 : 1 molar ratio of the hydride (crosslinker) to the vinyl group (SR) at room temperature. The requirement of such inhibitor is to increase the work life of the composite at ambient temperature by reducing the rate of crosslinking.[20] As a result, a crosslinking network formed between the SR and crosslinker through a hydrosilylation reaction,[21] as shown in Scheme 1. The thixotropic product so formed was outgassed and transferred to a Teflon Petri dish and was subjected to curing at 165°C for 15 min. The SR nanocomposite sheets, approximately 2 mm thick, were formed by postcuring at 200°C for 4 h in a hot-air oven. The same methodology was adopted for the preparation of sheets of neat SR.

Characterization

Fourier transform infrared (FTIR) spectra of DS–LDH, SR, and SR/DS–LDH (5 wt %) nanocomposites were recorded with a PerkinElmer RXI FTIR spectrometer (USA) over the wave-number range of 400–4000 cm^{-1}. The changes in the gallery distance of DS–LDH and its SR nanocomposites were measured with small-angle X-ray diffraction (SAXD) at room temperature in the range of 2–10° on a

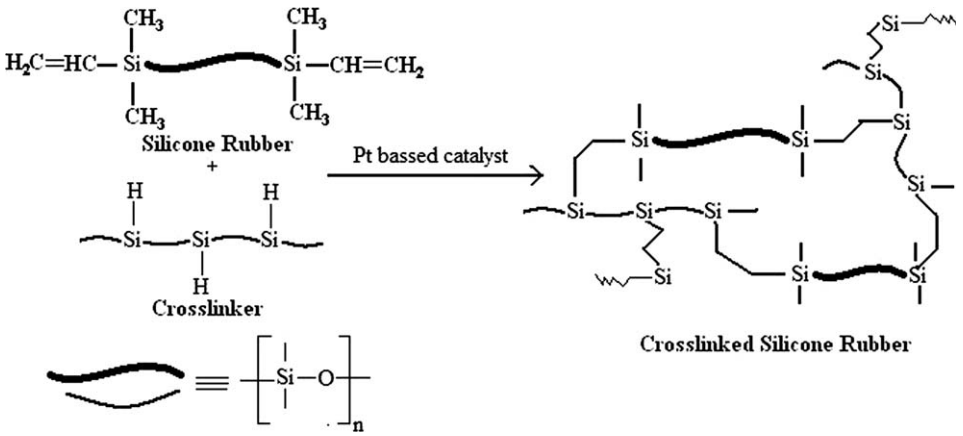

Scheme 1 Schematic presentation of the hydrosilylation reaction forming the crosslinked silicone elastomer.

PANalytical PW3040/60 X'Pert Pro (Holland) with Cu Kα radiation (wavelength = 0.1542 nm) at a scanning rate of 3°/min. The nature of the dispersion of DS–LDH in the SR matrix was analyzed with a JEOL 2100 200-kV transmission electron microscope (Japan). The sample for this purpose was prepared via the ultramicrotoming of the neat SR and SR/DS–LDH nanocomposites in the form of 80–100-nm-thick slices cut at −150°C with a diamond knife. Tensile properties were measured on a Tinius Olsen h10KS (UK) according to ASTM D 412-98 at room temperature with a crosshead speed of 300 mm/min^{-1}. The samples were prepared in a standard dumbbell shape; all measurements were repeated five times, and the values were averaged. The morphology of the gold-coated, tensile-fractured surface was recorded with a JEOL JSM-5800 scanning electron microscope with an acceleration voltage of 20 kV. Thermogravimetric analysis (TGA) was carried out with a PerkinElmer Redcroft 870 thermal analyzer at a heating rate of 10°C/min over a temperature range of 50–800°C in an N_2 atmosphere with an initial weight of approximately 5 mg for each sample. Differential scanning calorimetry (DSC) studies were performed with a PerkinElmer Pyris instrument at a heating rate of 10°C/min under an N_2 atmosphere. The solvent-uptake capacity of the nanocomposites was determined at 25°C in toluene with a gravimetric method (ASTM D 471-98).

RESULTS AND DISCUSSION

Infrared (IR) analysis

Figure 1 shows FTIR spectra of DS–LDH, SR, and the SR/DS–LDH (5 wt %) nanocomposite. A broad absorption band over the range of 3700–3000 cm^{-1} with a peak maximum around 3506 cm^{-1} was due to O—H stretching of hydroxyl groups of DS–LDH. However, for its nanocomposite with SR, this peak shifted to 3461 cm^{-1}. This was possibly due to the interaction between the DS–LDH layers and SR chains.[18] The absorption peak for the C—H stretching vibration of the SR/DS–LDH nanocomposite at 2906 cm^{-1} was more intense than that of the neat SR. In addition, the characteristic absorption peaks induced by Si—O—Si in SR at 1096 and 1025 cm^{-1} shifted to 1108 and 1020 cm^{-1}, respectively. Such behavior suggests the existence of hydrogen-bond interactions between the main chain of SR and DS–LDH layers and is in line with the observations of previous workers.[18,22]

XRD study

The SAXD patterns of DS–LDH, neat SR, and their nanocomposites with various loadings of DS–LDH are shown in Figure 2. In the case of DS–LDH, the diffraction peak was observed at 2θ = 3.19°. This corresponded to an interlayer distance (d_{003}) equivalent to 2.77 nm, which was almost 4 times higher than that of the pristine LDH basal spacing. According to the literature,[23] the chain length and sheet thickness of dodecyl sulfate (DS) and LDH

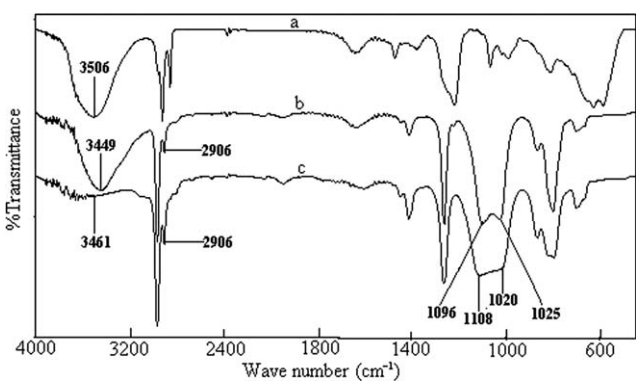

Figure 1 FTIR spectra for samples of (a) DS–LDH, (b) neat SR, and (c) the SR/DS–LDH (5 wt %) nanocomposite.

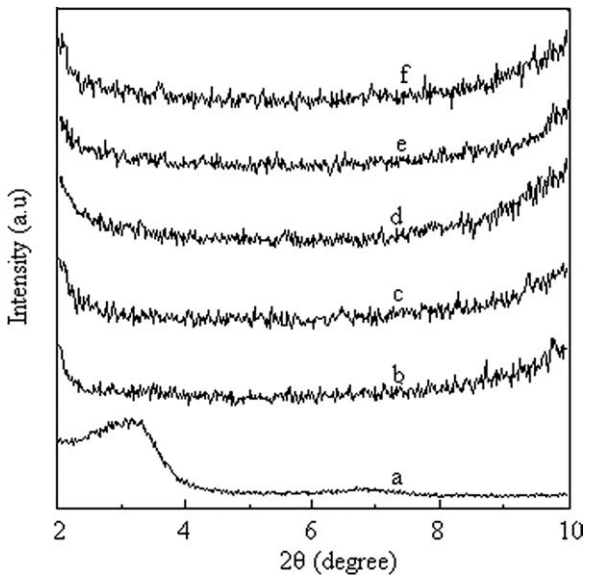

Figure 2 XRD spectra of (a) DS–LDH, (b) neat SR, and (c) SR/DS–LDH (1 wt %), (d) SR/DS–LDH (3 wt %), (e) SR/DS–LDH (5 wt %), and (f) SR/DS–LDH (8 wt %) nanocomposites.

individually are 2.07 and 0.48 nm, respectively. Therefore, the expanded basal spacing of approximately 2 nm between the LDH layers indicated that the DS molecules were intercalated into the LDH interlayer by an anion-exchange reaction, as illustrated in Scheme 2. This diffraction peak of DS–LDH disappeared for the SR nanocomposites with DS–LDH loadings of 1, 3, 5, and 8 wt %. This was due to the loss of structure registry in the stacking direction of the hydroxide layers, which indicated the possible formation of exfoliated hydroxide layers dispersed in the SR matrix on a nanometer scale. A network structure formed during the crosslinking process, in which the crosslinker reacted with the vinylic group of SR (Scheme 1). IR studies also established earlier that hydrogen-bond interactions existed between the polymer and —OH groups of the DS–LDH layers, and this possibly contributed to the exfoliation of the DS–LDH layers in the polymer matrix;[18] exfoliated SR/DS–LDH nanocomposites are proposed according to Scheme 3. The absence of the characteristic d_{003} peak of DS–LDH in SAXD for all the nanocomposites indicated the uniform

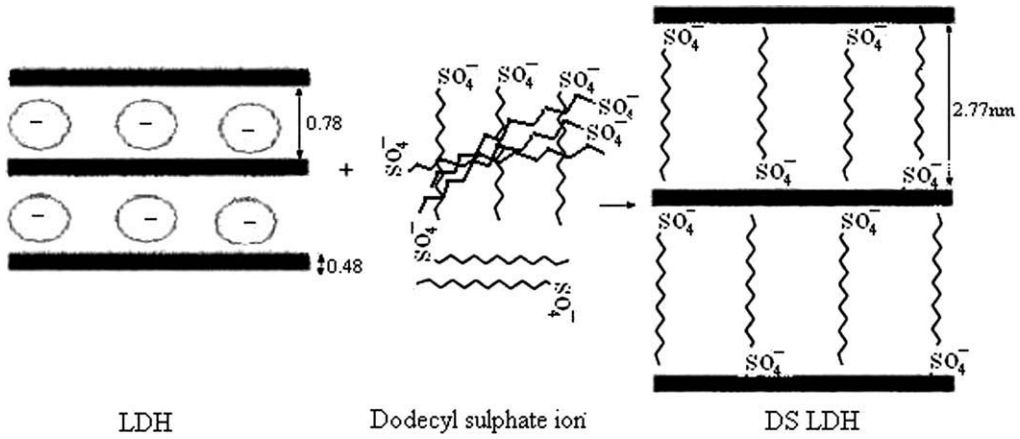

Scheme 2 Schematic diagram of pure LDH and DS–LDH.

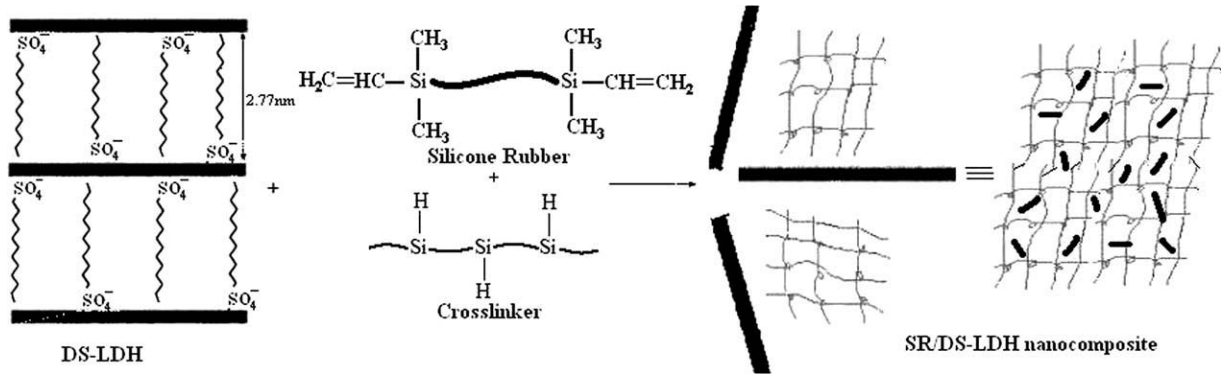

Scheme 3 Scheme of the intercalation process between DS–LDH and the SR matrix.

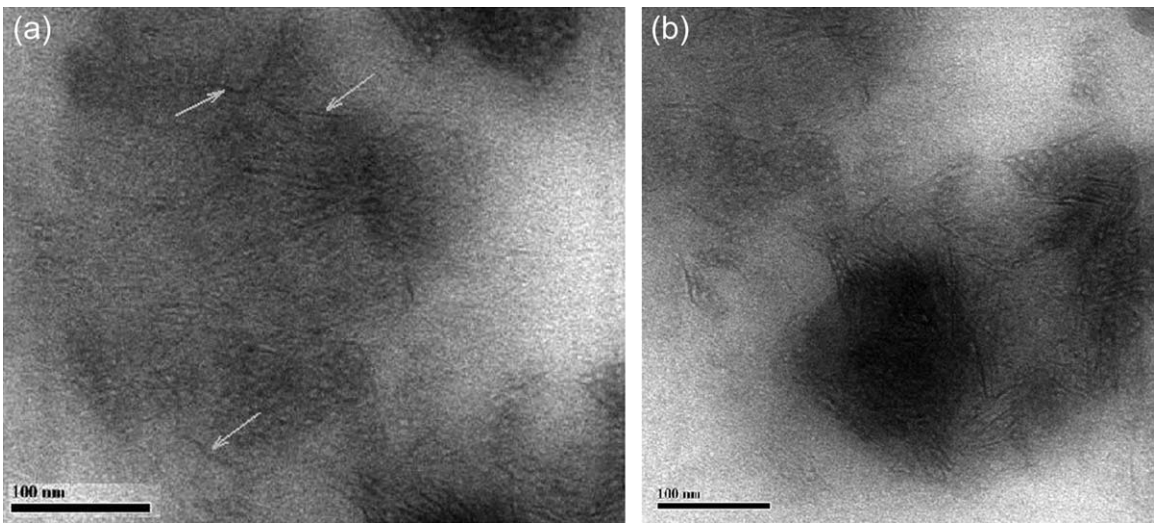

Figure 3 TEM images of (a) SR/DS–LDH (5 wt %) and (b) SR/DS–LDH (8 wt %) nanocomposites.

dispersion of nanofillers but did not confirm the formation of exfoliated nanocomposites. Therefore, a complete characterization of the nanocomposite morphology required investigation by microscopy.

TEM analysis

The TEM technique was used to confirm the exfoliated dispersion of LDH nanolayers in the polymer matrix. Figure 3(a) shows that the DS–LDH layers were well dispersed in the SR matrix with the 5 wt % filler loading, and this confirmed the formation of exfoliated nanocomposites. The positions indicated by arrows in Figure 3(a) also suggested that most of the exfoliated DS–LDH nanolayers were tilted with respect to the cutting section of the TEM specimen.[1] This observation is contrary to polymer/layered silicate exfoliation nanocomposites, in which the exfoliated clay layers often have a face–face orientation because of the high aspect ratio of approximately 100.[24] The thickness and length of the individual exfoliated DS–LDH layers were about 1.5–2.5 and 30–80 nm, respectively, and they corresponded to an aspect ratio of approximately 10. The TEM image provides positive evidence for the nanoscale dispersion of DS–LDH layers in the SR matrix. However, with an 8 wt % filler loading, some degree of aggregation was observed because of partial exfoliation of the SR chains in the gallery of DS–LDH, as shown in Figure 3(b).

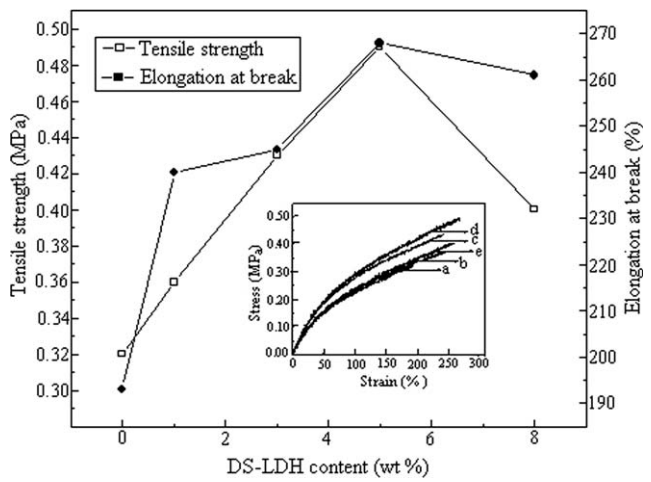

Figure 4 Variation of TS and EB with the DS–LDH contents for the SR/DS–LDH nanocomposites.

Mechanical properties

Figure 4 shows the effect of DS–LDH on the mechanical properties of SR. According to this, the tensile strength (TS) increased with increasing DS–LDH content in SR and was maximum with the 5 wt % DS–LDH loading; it was 53% higher than that of the pure SR. This enhanced TS was mainly due to the interaction between the Si—O polar groups of SR and the —OH functionality of DS–LDH; this was also supported by the IR studies discussed earlier. Interestingly, the elongation at break (EB) gradually increased with the DS–LDH content and was 38% higher for the SR/DS–LDH (5 wt %) nanocomposite versus the neat SR. Such improvement in TS and EB

TABLE I
Mechanical Properties of Neat SR and SR/DS–LDH Nanocomposites

LDH content (wt %)	TS (MPa)	EB (%)	Young's modulus (MPa)	Toughness (MJ/m^3)
0	0.32	193	0.32	0.395
1	0.36	240	0.39	0.588
3	0.43	245	0.44	0.678
5	0.49	268	0.49	0.845
8	0.40	261	0.41	0.668

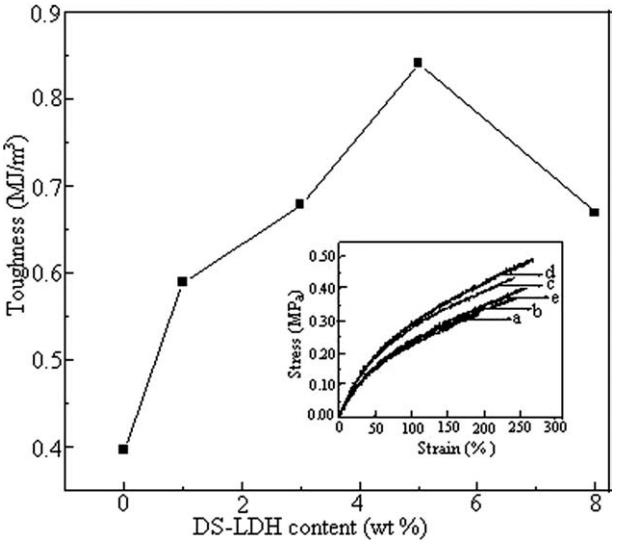

Figure 5 Toughness of the SR/DS–LDH nanocomposites with different weight percentages of DS–LDH.

may be attributed to the platelet orientation or chain slippage of DS–LDH in the SR matrix.[25] Moreover, the observed improvement in TS was comparable to that for SR/organomontmorillonite and SR/aerosilica, whereas EB was doubled with respect to that for SR/aerosilica nanocomposites.[15] The Young's modulus data in Table I follow a trend similar to that for TS; the maximum Young's modulus was found for the SR/DS–LDH (5 wt %) nanocomposite, and it was 42% higher than that for the pure SR. Toughness is the energy per unit of volume before fracture, and it can be calculated with the area underneath the stress–strain curve, which quantifies the work expended in deforming the material. Figure 5 shows that the toughness of the SR/DS–LDH nanocomposites increased with the filler loading increasing up to 5 wt % and then decreased. Such behavior can be attributed to the interaction between the DS–LDH layer and SR. However, the observed reductions in the TS, EB, and toughness values of the SR/DS–LDH nanocomposites at a higher filler loading were due to the aggregation of DS–LDH in nanocomposites and reduced the filler–matrix interactions.[16]

Fracture surface morphology

Figure 6(a,b) displays SEM micrographs of tensile-fractured surfaces of SR and its nanocomposites containing 5 wt % DS–LDH. The SEM images clearly show the presence of a larger smooth area for neat SR. They also indicate uniform failure of the SR matrix without any mechanically weaker region for crack initiation. However, when 5 wt % DS–LDH was added to SR, the surface was roughly fractured with a large number of microvoids [indicated by the arrow in Fig. 6(b)] around the dispersed nanoparticles. This may be attributed to the entrapment of a considerable amount of the polymer matrix within the particle clusters,[26] which absorbed energy during deformation and led to the maximum improvements in the mechanical properties of the polymer/LDH nanocomposites. These results indicated secondary cracks at the organic–inorganic interface and fracture steps before unification with the propagating primary crack.[27] The rough surface morphology of the SR polymer nanocomposites also accounted for the better mechanical properties similar to those of many other organic polymer nanocomposites.[28]

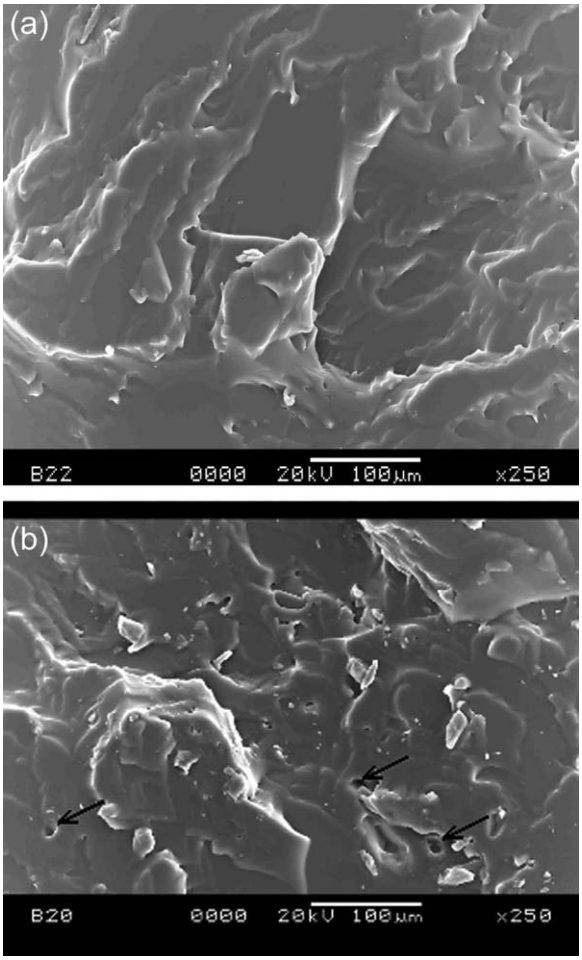

Figure 6 SEM images of the tensile fracture surface morphology of (a) neat SR and (b) the SR/DS–LDH (5 wt %) nanocomposite.

TGA

The thermal stability of SR is superior to that of many synthetic rubbers such as ethylene–propylene–diene monomer rubber and polyurethane. However, because of the presence of an inorganic siloxane (—Si—O—) backbone and the helical structure of the flexible main chain, SR decomposed into volatile cyclic silicones above 300°C.[29] Figure 7 shows the

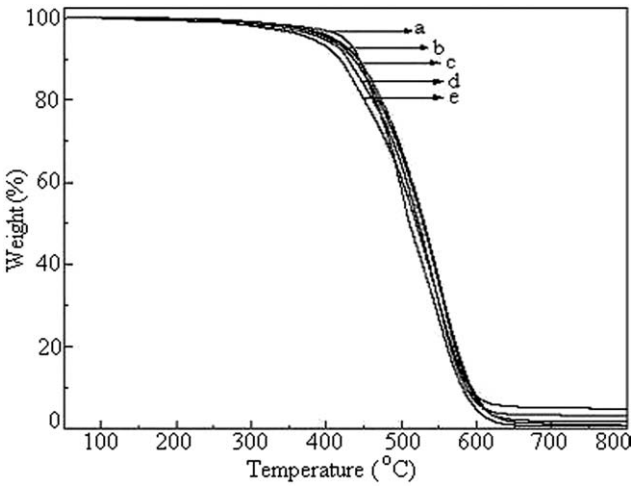

Figure 7 TGA profiles of the SR/DS–LDH nanocomposites with (a) 0, (b) 1, (c) 3, (d) 5, and (e) 8 wt % DS–LDH.

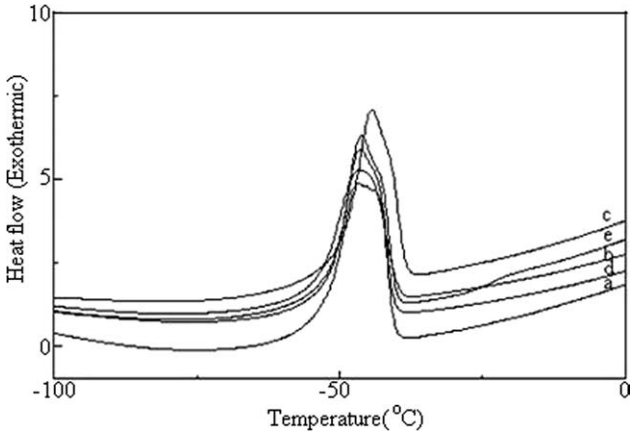

Figure 8 DSC curves of (a) neat SR and (b) SR/DS–LDH (1 wt %), (c) SR/DS–LDH (3 wt %), (d) SR/DS–LDH (5 wt %), and (e) SR/DS–LDH (8 wt %) nanocomposites.

TGA curves of the neat SR and its nanocomposites with different loadings of the DS–LDH filler, and the data related to the thermal degradation temperatures corresponding to the onset of degradation (T_0), 10% weight loss (T_{10}), and 50% weight loss (T_{50}) are recorded in Table II. TGA shows that both T_0 and T_{10} for all SR/DS–LDH nanocomposites were lower than those for the neat SR. This may be due to the dehydration of Mg–Al hydroxide sheets and thermal degradation of DS alkyl chains.[1] On the contrary, when 50% weight loss was selected as a point of comparison, the thermal degradation temperatures (T_{50}) for pure SR and SR/DS–LDH nanocomposites containing 1, 3, 5, or 8 wt % DS–LDH were 510.7, 530.3, 528.9, 523, and 519.8°C, respectively. This indicated that the thermal degradation temperature of the SR/DS–LDH nanocomposites was approximately 9–20°C higher with respect to the neat SR, the maximum improvement being 20°C for a 1 wt % LDH loading. This was higher than that of SR/organomontmorillonite and SR/aerosilica nanocomposites.[15] TGA curves also showed that the degradation rate at the midpoint was much slower than that of the pure SR. This may be due to the hindering effect of dispersed DS–LDH nanolayers, which prevented the diffusion of nitrogen and tended to reduce the rate of initiation of polymer chain scission to produce small, volatile products.[30] However, at the higher loading of DS–LDH (8 wt %), the thermal stability of these nanocomposites decreased because the relatively large DS contents of the composites produced less stable charred layers during the decomposition. Another possible reason is aggregation of LDH layers, which could have led to the formation of the heat source domains in the degradation step.[31] Table II shows that the percentage residue of these nanocomposites increased with increasing filler contents in SR. However, the amount of residue was higher than what was expected on the basis of the DS–LDH content only. This might have been due to the charring of the polymer, which consisted of carbonaceous char, silicon dioxide, and MgO and Al_2O_3 residue.[32]

DSC measurement

The crystal properties of pure SR and SR/DS–LDH nanocomposites were studied with DSC; the findings are displayed in Figure 8, and the data inferred from them are tabulated in Table I. The melting temperature (T_m) of neat SR was −46.76°C. The addition of DS–LDH nanofillers to SR increased T_m, and its value was maximum with a 3 wt % filler loading. This may be attributed to the homogeneously dispersed DS–LDH layers in the SR matrix, which

TABLE II
TGA and DSC Data for Neat SR and SR/DS–LDH Nanocomposites

LDH content (wt %)	T_0 (°C)	T_{10} (°C)	T_{50} (°C)	Residue at 700°C (wt %)	T_m (°C)	Enthalpy of crystallization (J/g)	Degree of crystallinity (%)
0	418	444	510.7	0.8	−46.76	23.7542	63.46
1	412	442	530.3	1.2	−46.38	23.8413	63.69
3	404	436	528.9	1.8	−44.27	24.4697	65.37
5	390	428	523.0	3.3	−46.42	23.7173	63.36
8	368	418	519.8	5.1	−46.26	23.1024	61.72

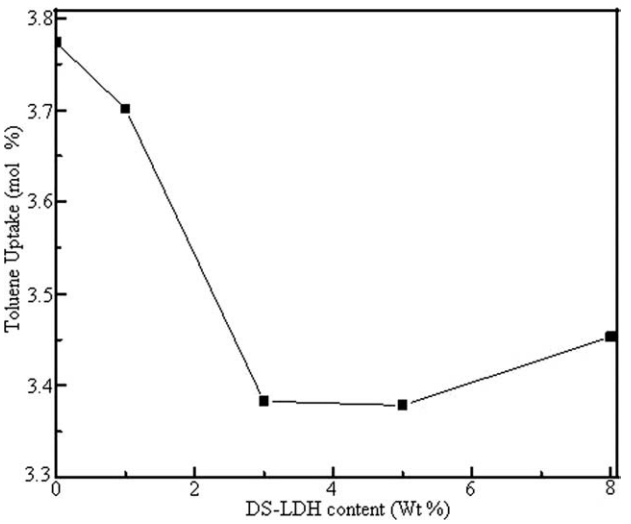

Figure 9 Influence of the DS–LDH content on the toluene uptake (mol %) of the SR/DS–LDH nanocomposites.

restricted the mobility of the polymer chains. This also implies that exfoliated DS–LDH layers might serve as nucleating agents with a strong heterogeneous effect on the crystallinity of the SR matrix.

The degree of crystallinity (crystallinity percentage) of the pure SR and SR/DS–LDH nanocomposites was determined as follows:

$$\text{Crystallinity } (\%) = \Delta H/\Delta H_{th}$$

where ΔH is the enthalpy of crystallization calculated via DSC for each sample and ΔH_{th} is the enthalpy of fusion of SR (37.43 J/g).[33] The degree of crystallinity for neat SR was 63.4%, and it increased with up to 3 wt % DS–LDH. This increase in the crystallinity of pure SR in the presence of DS–LDH may be attributed to the strong interaction between SR and DS–LDH layers, which in turn probably forced polymer chains to orient in a regular manner.[15,34] At a higher filler loading, the crystallinity of SR decreased because the crystal domains of the polymer chains were affected by DS–LDH layers.

Swelling properties

Solvent uptake depends on the filler reinforcing strength, which depends on the filler surface area and agglomerate structure. To understand more about SR/DS–LDH nanocomposites, the degree of polymer–filler interaction was calculated from equilibrium swelling in solvents with the Flory–Rehner equation.[34] Figure 9 shows the influence of DS–LDH on the toluene-uptake properties of pure SR and SR/DS–LDH nanocomposites. The solvent-uptake capacity decreased from the surface to the bulk region of the SR nanocomposites with up to a 5 wt % filler loading of DS–LDH. Such behavior has also been observed for SR/montmorillonite,[16] SR/nanosilica,[17] and so forth. This may be attributed to the strong interaction between SR and DS–LDH (forming a bound polymer) and polymer chains in close proximity to the reinforcing filler (DS–LDH), which was either physisorbed or chemisorbed to restrict the solvent uptake.[35] Alternatively, there is the possibility that the solvent-resistance properties of the SR/DS–LDH nanocomposites increased up to a 5 wt % filler loading because of the excellent barrier properties of the high-aspect-ratio (ca. 10) DS–LDH layers and the exfoliated structure of DS–LDH, which maximized the available surface area of the reinforcing phase. Therefore, the exfoliated structure and large surface area of the DS–LDH layers (251 m^2/g)[36] were favorable to the solvent-resistance properties of the SR/DS–LDH nanocomposites. However, at higher DS–LDH loadings, an increase in the solvent uptake was observed because of the aggregation of DS–LDH layers in the polymer matrix.

CONCLUSIONS

Exfoliated SR/DS–LDH nanocomposites were successfully prepared by the solution intercalation of SR in DS–LDH. XRD and TEM analysis confirmed that the dispersion of DS–LDH nanolayers (30–80 nm long) was homogeneous throughout the polymer matrix. The maximum improvements in TS (53%) and EB (38%) were achieved for the SR/DS–LDH (5 wt %) nanocomposites. The thermal stability of the SR/DS–LDH nanocomposites increased by approximately 9–20°C in comparison with neat SR. DSC analysis showed that T_m of the SR/DS–LDH (3 wt %) nanocomposites (−44.27°C) was higher than that of neat SR (−46.76°C). Swelling property analysis confirmed improvements in the solvent resistance of the SR/DS–LDH nanocomposites with respect to the neat polymer.

References

1. Chen, W.; Qu, B. Chem Mater 2003, 15, 3208.
2. Kuila, T.; Acharya, H.; Srivastava, S. K.; Bhowmick, A. K. Polym Compos 2008, 30, 497.
3. Pramanik, M.; Srivastava, S. K.; Samantaray, B. K.; Bhowmick, A. K. J Polym Sci Part B: Polym Phys 2002, 40, 2065.
4. Acharya, H.; Pramanik, M.; Srivastava, S. K.; Bhowmick, A. K. J Appl Polym Sci 2004, 93, 2429.
5. Pramanik, M.; Srivastava, S. K.; Samantaray, B. K.; Bhowmick, A. K. J Appl Polym Sci 2003, 87, 2216.
6. Alexandre, M.; Dubois, P. Mater Sci Eng 2000, 28, 1.
7. Srivastava, S. K.; Pramanik, M.; Acharya, H. J Polym Sci Part B: Polym Phys 2006, 44, 471.
8. Meyn, M.; Beneke, K.; Lagaly, G. Inorg Chem 1990, 29, 5201.
9. Dékány, I.; Berger, F.; Imrik, K.; Lagaly, G. Colloid Polym Sci 1997, 275, 681.
10. Bhattacharjee, S.; Anderson, J. A. Chem Commun 2004, 5, 554.

11. Braterman, P. S.; Xu, Z. P.; Yarberry, F. In Layered Double Hydroxides; Auerbach, S. M.; Carrado, K. A.; Dutta, P. K., Eds.; Marcel Dekker: New York, 2004; p 373.
12. Chibwe, K.; Jones, W. Chem Commun 1989, 14, 926.
13. Bhowmick, A. K.; Stephens, H. L. Handbook of Elastomers; Marcel Dekker: New York, 2001; p 605.
14. Chiu, H. T.; Wu, J. H. J Appl Polym Sci 2005, 97, 711.
15. Wang, J.; Chen, Y.; Jin, Q. Macromol Chem Phys 2005, 206, 2512.
16. Burnside, S. D.; Giannelis, E. P. J Polym Sci Part B: Polym Phys 2000, 38, 1595.
17. Dewimille, L.; Bresson, B.; Bokobza, L. Polymer 2005, 46, 4135.
18. Wen, J.; Li, Y.; Zuo, Y.; Zhou, G.; Li, J.; Jiang, L.; Xu, W. Mater Lett 2008, 62, 3307.
19. Carlino, S. Solid State Ionics 1997, 98, 73.
20. Bobear, W. J.; Latham, N. Y. U.S. Pat. 4,061,609 (1977).
21. Brook, M. A. Biomaterials 2006, 27, 3274.
22. Fujiki, M.; Saxena, A. J Polym Sci Part A: Polym Chem 2008, 46, 4637.
23. Sundell, S. Acta Chem Scand A 1977, 31, 799.
24. Triantafillidis, C. S.; LeBaron, P. C.; Pinnavaia, T. J. Chem Mater 2002, 14, 4088.
25. Wu, Y. P.; Ma, Y.; Wang, Y. Q.; Zhang, L. Q. Macromol Mater Eng 2004, 289, 890.
26. Costa, F. R.; Satapathy, B. K.; Wagenknecht, U.; Weidisch, R.; Heinrich, G. Eur Polym J 2006, 42, 2140.
27. Wetzel, B.; Haupert, F.; Zhang, M. Q. Compos Sci Technol 2003, 63, 2055.
28. The, P. L.; Ishak, Z. A. M.; Hashim, A. S.; Kocsis, J. K.; Ishiaku, U. S. Eur Polym J 2004, 40, 2513.
29. Grassie, N.; Macfarlane, I. G. Eur Polym J 1978, 14, 875.
30. Brunside, S. D.; Giannelis, E. P. Chem Mater 1995, 7, 1597.
31. Chen, W.; Qu, B. J Mater Chem 2004, 14, 1705.
32. Timpe, D. C., Jr. Technical Detail: "Formaldehyde generation from silicone rubber" Arlon Silicone Technologies Division.
33. Aranguren, M. I. Polymer 1998, 39, 4897.
34. Kuila, T. Ph.D. Thesis, Indian Institute of Technology, 2009.
35. Huang, J. C.; Zhu, Z. K.; Yin, J.; Qian, X.-F.; Sun, Y. Y. Polymer 2001, 42, 873.
36. Corma, A.; Iborra, S.; Miquel, S.; Primo, J. J Catal 1998, 173, 315.